

## Quantum error correction beyond qubits

Takao Aoki<sup>1</sup>, Go Takahashi<sup>1,2</sup>, Tadashi Kajiyama<sup>1,2</sup>  
 Jun-ichi Yoshikawa<sup>1,2</sup>, Samuel L. Braunstein<sup>3</sup>,  
 Peter van Loock<sup>4</sup> & Akira Furusawa<sup>1,2</sup>

<sup>1</sup>Department of Applied Physics, School of Engineering, The University of Tokyo, 7-3-1 Hongo, Bunkyo-ku, Tokyo 113-8656, Japan

<sup>2</sup>CREST, Japan Science and Technology (JST) Agency, 1-9-9 Yaesu, Chuo-ku, Tokyo 103-0028, Japan

<sup>3</sup>Computer Science, University of York, York YO10 5DD, UK

<sup>4</sup>Optical Quantum Information Theory Group, Institute of Theoretical Physics I and Max-Planck Research Group, Institute of Optics, Information and Photonics, Universität Erlangen-Nürnberg, Staudtstr. 7/B2, 91058 Erlangen, Germany

**Quantum computation and communication rely on the ability to manipulate quantum states robustly and with high fidelity. Thus, some form of error correction is needed to protect fragile quantum superposition states from corruption by so-called decoherence noise. Indeed, the discovery of quantum error correction (QEC)<sup>1,2</sup> turned the field of quantum information from an academic curiosity into a developing technology. Here we present a continuous-variable experimental implementation of a QEC code, based upon entanglement among 9 optical beams<sup>3</sup>. In principle, this 9-wavepacket adaptation of Shor's original 9-qubit scheme<sup>1</sup> allows for full quantum error correction against an arbitrary single-beam (single-party) error.**

QEC protocols eliminate uncontrolled errors that affect fragile quantum superposition states by encoding these quantum states into a larger, multi-partite entangled system. Errors occurring on a limited number of parties will leave the entanglement intact and so the original state may be retrieved by error syndrome recognition followed by recovery operations. Shor proposed a concatenated quantum code to protect against arbitrary single-qubit errors, by encoding an arbitrary single-qubit state  $|\psi\rangle = \alpha|0\rangle + \beta|1\rangle$  into nine physical qubits

$$|\psi_{\text{encode}}\rangle = \alpha|+, +, +\rangle + \beta|-, -, -\rangle, \quad (1)$$

with  $|\pm\rangle = (|0, 0, 0\rangle \pm |1, 1, 1\rangle)/\sqrt{2}$ . Though reminiscent of the redundant encoding in classical error correction, the quantum code exhibits some clearly nonclassical features of which the most significant is the presence of multi-party entanglement. The concatenation of three-party entangled states ( $|\pm\rangle$ ) into nine-party states enables one to correct both bit-flip and phase-flip errors. The latter type of error occurs only in nonclassical states. Remarkably, suitable error syndrome measurements would collapse an *arbitrary* error (including coherent superpositions of bit-flip and phase-flip errors) into the discrete set of only bit-flip and/or phase-flip errors. These discrete (Pauli) errors can be easily reversed to recover the original state.

The continuous-variable version of Shor's 9-qubit code<sup>1,3</sup> is the only code to date which can be deterministically (unconditionally) implemented using only linear optics and sources of entanglement. Indeed, previous implementations of QEC were based on qubit codes, either in liquid-state NMR or linear ion trap hardware configurations. The liquid-state NMR experiments implemented QEC codes with up to five physical qubits<sup>4,5,6,7</sup> and in the ion trap experiment, a three-qubit code was realized<sup>8</sup>. Both configurations rely on nonlinear qubit-qubit coupling (in the form of nearest-neighbor couplings for NMR or via the collective vibrational mode for ion traps). Our experiment is the first implementation of a Shor-type code, as the preparation of nine-party entanglement is still beyond the scope of existing non-optical approaches and single-photon-based, optical schemes. Here, continuous-variable QEC<sup>9,10</sup> is realized using squeezed states of light and networks of beam splitters<sup>3</sup>. Even this optical approach requires an optical network three times the size as that used in earlier experiments<sup>11</sup> to achieve the large-scale multi-partite entanglement for a 9-wavepacket code.

In our scheme, as for the simplest QEC codes (whether for qubits or for continuous variables), a single, arbitrary error can be corrected. Such schemes typically assume errors occur stochastically and therefore rely on the low frequency of multiple errors. Stochastic error models may describe, e.g., stochastic, depolarizing channels for qubits, or in the continuous-variable regime<sup>13,14</sup>, free-space channels with atmospheric fluctuations causing beam jitter, as considered recently for various non-deterministic distillation protocols<sup>16,17,18,19</sup>. For the continuous-variable QEC protocols, as realized in the present work, this type of error may be suppressed in a *deterministic* fashion (see appendix F). The overall performance of this family of QEC codes is then only limited by the accuracy with which ancilla state preparation, encoding and decoding circuits, and syndrome extraction and recovery operations can be achieved. In the continuous-variable scheme, all these ingredients can be highly efficiently implemented; the finite squeezing of the auxiliary modes being the only limitation. This ancilla squeezing is linked with the presence of entanglement and it also determines whether the transfer fidelities exceed those of classical error correction (see appendices E and F).

We begin with a description of the scheme in the limit of infinite squeezing, where the position  $x$  and momentum  $p$  of a harmonic oscillator (corresponding to a single optical mode of the light field) serve as the conjugate pair of observables used for the encoding

$$|\psi_{\text{encode}}\rangle = \int dP \psi(P) |P, P, P\rangle, \quad (2)$$

with  $|P\rangle = \frac{1}{\sqrt{\pi}} \int dx e^{2ixP} |x, x, x\rangle$ , units-free for  $\hbar = \frac{1}{2}$ . Through this 9-wavepacket code an arbitrary single-mode state  $|\psi\rangle = \int dx \psi(x)|x\rangle$  is encoded into nine optical modes. This perfectly encoded state is obtained by using

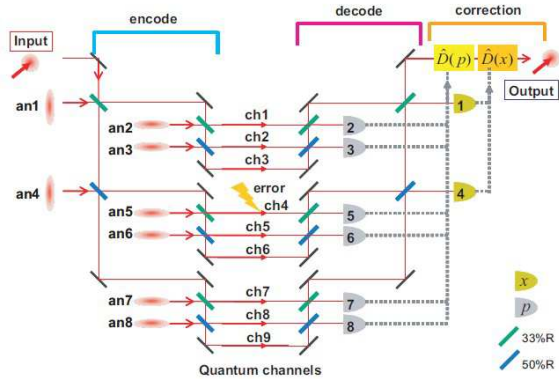


FIG. 1: 9-wavepacket quantum error correction code<sup>3</sup> for correcting an arbitrary error occurring in any one of the nine channels. The gray dotted lines represent the classical information that is used to compute the necessary syndrome recovery operations.

eight infinitely squeezed ancilla states. Finite squeezing of the ancillae leads to an approximate encoding, and hence lowers the fidelity of the QEC.

Fig. 1 shows a schematic of our realization of the 9-wavepacket code. In the encoding stage, an input state is entangled with eight squeezed ancillae, each corresponding to an approximate ‘0’ (“blank”) state. After an error is introduced, the states are decoded simply by inverting the encoding. The eight ancilla modes are then measured (with  $x$ -quadrature measurements performed in detectors 1 and 4 and  $p$ -quadrature measurements in six other detectors), and the results of the measurement are used for error syndrome recognition. More precisely, these are the results of homodyne detection applied to the ancilla modes along their initial squeezing direction.

The encoding stage consists of two steps in order to realize the concatenation of position and momentum codes<sup>3</sup>. First, position-encoding is achieved via a *tritter*  $T_{in,an1,an4}$ , that is two beam splitters (blue and green in Fig. 1) acting upon the input mode and two  $x$ -squeezed ancilla modes (an1 and an4 in Fig. 1). The second step provides the momentum-encoding via three more tritters, with six additional  $p$ -squeezed ancilla modes (an2, an3, an5, an6, an7 and an8 in Fig. 1). The overall encoding circuit becomes<sup>20</sup>

$$T_{an4,an7,an8}T_{an1,an5,an6}T_{in,an2,an3}T_{in,an1,an4} \cdot \quad (3)$$

As the decoding stage merely inverts the encoding, the eight ancilla modes will remain all ‘0’ in the absence of errors. In the presence of an error in any one of the nine channels, the measurement results of the decoded ancillae will lead to non-zero components, containing sufficient information for identifying and hence correcting the error (see appendices for derivations and Table I for an error-syndrome map). Similar to the qubit QEC scheme, where the conditional state after the syndrome measure-

ments becomes the original input state up to some discrete Pauli errors, our conditional state coincides with the input state up to some simple phase-space displacements. Thus, it remains only to apply the appropriate (inverse) displacement operations in order to correct the errors.

The detailed experimental setup for our 9-wavepacket QEC scheme is shown in Fig. 2. Eight squeezed vacua are created by four optical parametric oscillators (OPOs), which have two counter-propagating modes; thus, every OPO creates two individual squeezed vacua. The squeezing level of each single-mode squeezed vacuum state corresponds to roughly 1 dB below shot noise. For pumping the OPOs, the 2nd harmonic of a cw Ti:Sapphire laser output is used. The syndrome measurements are performed via homodyne detection with near-unit efficiency.

To apply a single error, a coherent modulation is first generated in a so-called error beam using an electro-optic modulator (EOM) (“modulated mode”). This beam is then superimposed onto the selected mode or channel (“target mode”) through a high-reflectivity beam splitter<sup>21</sup> with independently swept phase, resulting in a quasi-random displacement error. The error-correcting displacement operations (as determined by decoding and measurement) are then performed similarly, via an EOM and a high-reflectivity beam splitter, but now with phase locking between the modulated and target modes along either the  $x$  or  $p$  axis, as appropriate.

TABLE I: Error syndrome measurements. LO phase: quadrature at which the local oscillator phase of the homodyne detector is locked, ES: equal signs, DS: different signs.

channel with an error	detectors with non-zero outputs	LO phase
1	1	$x$
	2	$p$
2	1	$x$
	2,3 (DS)	$p$
3	1	$x$
	2,3 (ES)	$p$
4	1,4 (DS)	$x$
	5	$p$
5	1,4 (DS)	$x$
	5,6 (DS)	$p$
6	1,4 (DS)	$x$
	5,6 (ES)	$p$
7	1,4 (ES)	$x$
	7	$p$
8	1,4 (ES)	$x$
	7,8 (DS)	$p$
9	1,4 (ES)	$x$
	7,8 (ES)	$p$

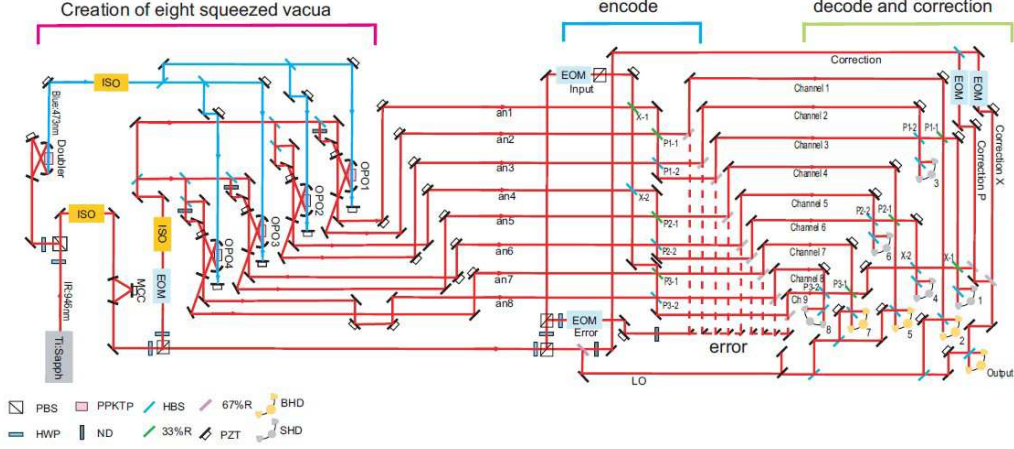


FIG. 2: Experimental setup of the 9-wavepacket quantum error correction; PBS: polarization beam splitter, PPKTP: periodically poled KTiOPO<sub>4</sub>, HBS: half (symmetric) beam splitter, HWP: half wave plate, ND: neutral density filter, PZT: piezoelectric transducer, BHD: balanced homodyning, SHD: self-homodyning, OPO: optical parametric oscillator, MCC: mode-cleaning cavity, LO: local oscillator, ISO: optical isolator, EOM: electro-optic modulator.

Fig. 3 shows some examples for error syndrome measurement results. Here, the input state is chosen to be

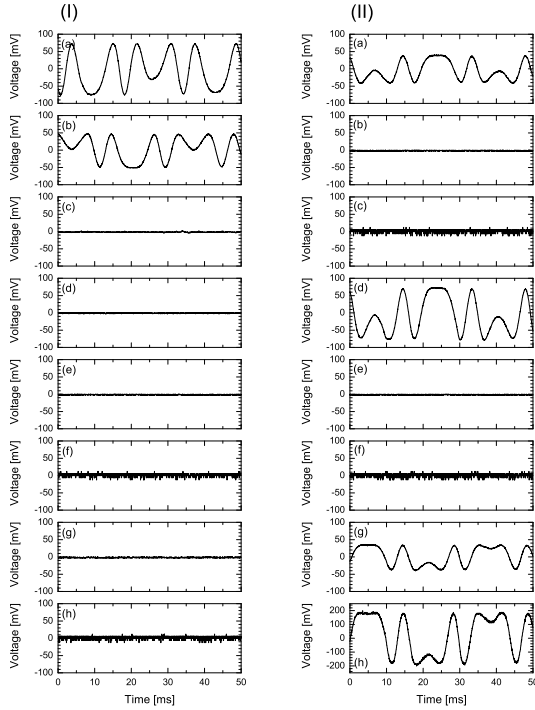


FIG. 3: Error syndrome measurement results. (I) A random displacement error is imposed on channel 1. (II) A random displacement error is imposed on channel 9. A two-channel oscilloscope is used measuring the outputs of detectors 1 and 4, 2 and 3, 5 and 6 and 7 and 8. (a) output signal of detector 1, (b) detector 2, (c) detector 3, (d) detector 4, (e) detector 5, (f) detector 6, (g) detector 7, (h) detector 8.

a vacuum state. A random displacement error in phase space is imposed on channel 1 (Fig. 3(I)) and on channel 9 (Fig. 3(II)). A two-channel oscilloscope is used to measure the outputs of pairs of detectors (1, 4), (2, 3), (5, 6), and (7, 8). Comparing the results of Fig. 3(I) with Table 1, one can identify an error occurring in channel 1, since only detectors 1 and 2 have non-zero outputs. The outputs from detectors 1 and 2 correspond to the desired  $x$  and  $p$  displacements, respectively. Similarly, from Fig. 3(II), we can recognize that an error has occurred in channel 9. Here, detectors 1, 4, 7, and 8 have non-zero outputs and the outputs of detectors 1 and 4, as well as 7 and 8 have equal signs (distinguishing it from the case of an error in channel 8, for which outcomes 7 and 8 have different signs).

Fig. 4 shows two examples of QEC results, comparing output states with and without error correction, and with and without squeezing of the ancilla modes. In Fig. 4(I), an error was introduced in channel 1. The local oscillator (LO) phase of the homodyne detector was tuned to detect the  $x$  quadrature of channel 1. Similarly, in Fig. 4(II), the error was introduced in channel 9 and the LO phase is locked to the  $p$  quadrature. For ease of experimental implementation, only the measurement outcomes of detectors 4 and 8 were fed forward to the error correction step. In principle, using the combined outputs of detectors 1 and 4 for  $x$  and detectors 7 and 8 for  $p$  would yield even higher fidelities.

The quality of the error correction can be assessed via the fidelity  $F = \langle \psi_{\text{in}} | \hat{\rho}_{\text{out}} | \psi_{\text{in}} \rangle$ , where  $|\psi_{\text{in}}\rangle$  represents the input state and  $\hat{\rho}_{\text{out}}$  corresponds to the output state of the error correction circuit<sup>21,22,23</sup>. Here the fidelity is calculated as

$$F = \frac{2}{\sqrt{(1 + 4\langle(\Delta\hat{x}_{\text{out}})^2\rangle)(1 + 4\langle(\Delta\hat{p}_{\text{out}})^2\rangle)}}, \quad (4)$$

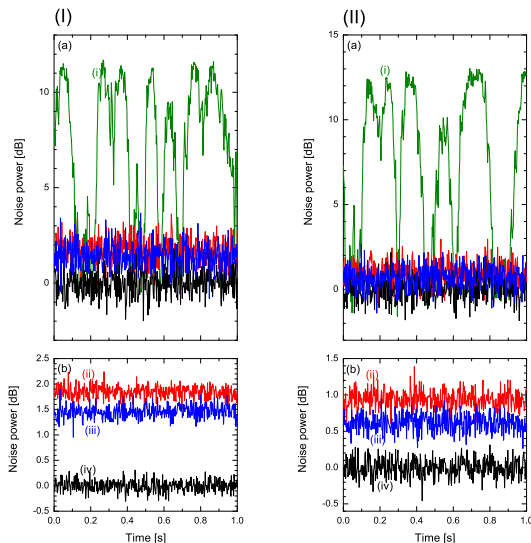


FIG. 4: Results of quantum error correction. (I) A random phase-space displacement error is imposed on channel 1. The LO phase of the homodyne detector is locked to the  $x$  quadrature. (II) A random displacement error is imposed on channel 9. The LO phase of the homodyne detector is locked to the  $p$  quadrature. In each case, four traces are shown comparison: (i) Homodyne detector output without error correction (no feed forward step). (ii) Error correction output without squeezing. (iii) Error correction output with squeezing. (iv) shot noise level. (a) Single scan of a spectrum analyzer with zero span mode. 2 MHz center frequency, 30 kHz resolution band width and 300 Hz video band width. (b) 30 times average of traces (ii-iv) above.

where  $\hat{x}_{\text{out}}$  and  $\hat{p}_{\text{out}}$  are quadrature operators of the output field. For example, in the case of an error in channel 1, the output quadrature operators become

$$\begin{aligned}\hat{x}_{\text{out}} &= \hat{x}_{\text{in}} - \frac{1}{\sqrt{2}}\hat{x}_{\text{an1}}^{(0)}e^{-r_1} \\ \hat{p}_{\text{out}} &= \hat{p}_{\text{in}} - \frac{1}{\sqrt{6}}\hat{p}_{\text{an2}}^{(0)}e^{-r_2},\end{aligned}\quad (5)$$

where  $\hat{x}_{\text{in}}$ ,  $\hat{p}_{\text{in}}$ ,  $\hat{x}_{\text{an1}}^{(0)}$ , and  $\hat{p}_{\text{an2}}^{(0)}$  are quadrature operators of the input field and the ancilla vacuum modes, and  $r_i$  are squeezing parameters for ancilla  $i$ . In the ideal case of  $r_i \rightarrow \infty$ , unit fidelity is obtained, with output states approaching the input states. For zero squeezing, Eq. (5) yields an excess noise of  $\frac{1}{2}$  and  $\frac{1}{6}$  for the  $x$  and  $p$  quadratures, corresponding to 1.76 dB and 0.67 dB of output powers, respectively (see Table II).

Eq. (4) can be used to translate the measured noise level values from Table II into fidelity values. Indeed, for every possible error introduced (in any of the channels) the fidelity after error correction exceeds the maximum values achievable for the scheme in the absence of ancilla squeezing. For example, for an error in mode 1, a fidelity of  $0.88 \pm 0.01$  was achieved (exceeding the classical cutoff of 0.86). Similarly, for an error in channel 9, we obtain

TABLE II: Output noise power of QEC circuit in dB, relative to the shot noise level. Perfect error correction therefore corresponds to 0 dB. SQV: squeezed vacua.

error on mode	quadrature of output	output power without SQV (theory)	output power without SQV (experiment)	output power with SQV (experiment)
1	$x$	1.76	$1.84 \pm 0.12$	$1.46 \pm 0.13$
	$p$	0.67	$0.68 \pm 0.12$	$0.57 \pm 0.12$
2	$x$	1.76	$1.75 \pm 0.12$	$1.42 \pm 0.13$
	$p$	0.87	$0.97 \pm 0.12$	$0.72 \pm 0.12$
3	$x$	1.76	$1.83 \pm 0.12$	$1.41 \pm 0.12$
	$p$	0.87	$0.92 \pm 0.12$	$0.70 \pm 0.12$
4	$x$	2.22	$2.26 \pm 0.12$	$1.67 \pm 0.12$
	$p$	0.67	$0.73 \pm 0.12$	$0.50 \pm 0.12$
5	$x$	2.22	$2.33 \pm 0.12$	$1.79 \pm 0.12$
	$p$	0.87	$0.88 \pm 0.12$	$0.73 \pm 0.13$
6	$x$	2.22	$2.34 \pm 0.12$	$1.77 \pm 0.12$
	$p$	0.87	$0.87 \pm 0.13$	$0.73 \pm 0.13$
7	$x$	2.22	$2.30 \pm 0.13$	$1.72 \pm 0.12$
	$p$	0.67	$0.69 \pm 0.12$	$0.57 \pm 0.12$
8	$x$	2.22	$2.18 \pm 0.13$	$1.79 \pm 0.13$
	$p$	0.87	$0.84 \pm 0.12$	$0.65 \pm 0.12$
9	$x$	2.22	$2.18 \pm 0.14$	$1.82 \pm 0.13$
	$p$	0.87	$0.94 \pm 0.12$	$0.61 \pm 0.12$

a fidelity of  $0.86 \pm 0.01$ , exceeding a cutoff of 0.82. (The lower cutoff takes into consideration that only two of the four non-zero components are used.) The better-than-classical fidelities for errors in *any* one of the nine channels are indirect evidence of entanglement-enhanced error correction (see appendices). By comparison, in complete absence of any error correction, i.e., without reversing displacement errors (including the zero-squeezing case; for an application of such ‘‘classical’’ error correction, see appendix F), fidelity values under  $0.007 \pm 0.001$  were obtained.

In conclusion, we experimentally demonstrated a Shor-type quantum error correction scheme based upon entanglement among nine optical beams. The entanglement is used for deterministically generating a concatenated code, allowing for the correction of arbitrary errors in any one of nine communication channels. In the experiment, evidence is obtained for an entanglement-enhanced correction of displacement errors; a further increase of the small enhancement of the current implementation would only require higher squeezing levels of the resource states. Our experiment represents the first demonstration of quantum error correction beyond qubits (and specifically for continuous variables). The scheme may be useful for any application in which stochastic errors occur such as free-space communication with fluctuating losses and beam pointing errors<sup>16,17,18,19</sup>. The ability to

implement QEC in an optical network of this size represents a significant step towards the manipulation and application of large-scale multi-partite entanglement for quantum information processing.

This work was partly supported by SCF and GIA com-

missioned by the MEXT of Japan. PvL acknowledges the DFG for funding under the Emmy Noether programme. AF acknowledges Y. Takeno for preparing the figures. TA's current address is PRESTO, Japan Science and Technology Agency (JST), Saitama, Japan.

- 
- <sup>1</sup> P. W. Shor, Phys. Rev. A **52**, R2493 (1995).  
<sup>2</sup> A. M. Steane, Phys. Rev. Lett. **77**, 793 (1996).  
<sup>3</sup> S. L. Braunstein, Nature **394**, 47 (1998).  
<sup>4</sup> D. G. Cory et al., Phys. Rev. Lett. **81**, 2152 (1998).  
<sup>5</sup> D. Leung, et al., Phys. Rev. A **60**, 1924 (1999).  
<sup>6</sup> E. Knill et al., Phys. Rev. Lett. **86**, 5811 (2001).  
<sup>7</sup> N. Boulant et al., Phys. Rev. Lett. **94**, 130501 (2005).  
<sup>8</sup> J. Chiaverini et al., Nature **432**, 602 (2004).  
<sup>9</sup> S. L. Braunstein, Phys. Rev. Lett. **80**, 4084 (1998).  
<sup>10</sup> S. Lloyd and J.-J. E. Slotine, Phys. Rev. Lett. **80**, 4088 (1998).  
<sup>11</sup> H. Yonezawa, T. Aoki and A. Furusawa, Nature **431**, 430 (2004).  
<sup>12</sup> M. A. Nielsen and I. L. Chuang, *Quantum Computation and Quantum Information* (Cambridge University Press, 2000).  
<sup>13</sup> P. van Loock, Los Alamos arXive quant-ph/0811.3616 (2008).  
<sup>14</sup> note that it was proven recently that quantum error correction of Gaussian errors for Gaussian signal states using Gaussian resources and Gaussian operations is impossible<sup>15</sup>; the error models referred to here<sup>13</sup> and discussed in the appendix correspond to non-Gaussian errors.  
<sup>15</sup> J. Niset, J. Fiurášek, and N. J. Cerf, Los Alamos arXive quant-ph/0811.3128 (2008).  
<sup>16</sup> J. Heersink et al., Phys. Rev. Lett. **96**, 235601 (2006).  
<sup>17</sup> R. Dong et al., Nature Physics, in press.  
<sup>18</sup> R. Schnabel et al., Nature Physics, in press.  
<sup>19</sup> J. Niset et al., Phys. Rev. Lett. **101**, 130503 (2008).  
<sup>20</sup> in the experiment, we generated a code state with position  $x$  and momentum  $p$  interchanged. This encoding (and the corresponding QEC protocol) involves only a change of basis with no drop in performance. Quantum optically, this change corresponds to a 90-degree rotation of the quadrature amplitudes, requiring local oscillator phases to be shifted by 90 degrees for homodyne detection.  
<sup>21</sup> A. Furusawa et al., Science **282**, 706 (1998).  
<sup>22</sup> S. L. Braunstein et al., Phys. Rev. A **64**, 022321 (2001).  
<sup>23</sup> K. Hammerer et al., Phys. Rev. Lett. **94**, 150503 (2005).  
<sup>24</sup> P. van Loock and A. Furusawa, Phys. Rev. A **67**, 052315 (2003).

## APPENDIX A: ENCODING

Equation (3) describes a nine-port device acting upon the signal input mode, two  $x$ -squeezed ancilla modes (“an1” and “an4” in Fig. 1 of main body), and six  $p$ -squeezed ancilla modes (“an2”, “an3”, “an5”, “an6”, “an7”, and “an8” in Fig. 1). Labeling the nine input modes by subscripts one through nine, we obtain the out-

put quadrature operators of the encoded state,

$$\begin{aligned}
 \hat{x}_1 &= \frac{1}{3}\hat{x}_{\text{in}} + \frac{\sqrt{2}}{3}\hat{x}_{\text{an1}}^{(0)}e^{-r_1} + \sqrt{\frac{2}{3}}\hat{x}_{\text{an2}}^{(0)}e^{r_2}, \\
 \hat{p}_1 &= \frac{1}{3}\hat{p}_{\text{in}} + \frac{\sqrt{2}}{3}\hat{p}_{\text{an1}}^{(0)}e^{r_1} + \sqrt{\frac{2}{3}}\hat{p}_{\text{an2}}^{(0)}e^{-r_2}, \\
 \hat{x}_2 &= \frac{1}{3}\hat{x}_{\text{in}} + \frac{\sqrt{2}}{3}\hat{x}_{\text{an1}}^{(0)}e^{-r_1} - \sqrt{\frac{1}{6}}\hat{x}_{\text{an2}}^{(0)}e^{r_2} \\
 &\quad + \sqrt{\frac{1}{2}}\hat{x}_{\text{an3}}^{(0)}e^{r_3}, \\
 \hat{p}_2 &= \frac{1}{3}\hat{p}_{\text{in}} + \frac{\sqrt{2}}{3}\hat{p}_{\text{an1}}^{(0)}e^{r_1} - \sqrt{\frac{1}{6}}\hat{p}_{\text{an2}}^{(0)}e^{-r_2} \\
 &\quad + \sqrt{\frac{1}{2}}\hat{p}_{\text{an3}}^{(0)}e^{-r_3}, \\
 \hat{x}_3 &= \frac{1}{3}\hat{x}_{\text{in}} + \frac{\sqrt{2}}{3}\hat{x}_{\text{an1}}^{(0)}e^{-r_1} - \sqrt{\frac{1}{6}}\hat{x}_{\text{an2}}^{(0)}e^{r_2} \\
 &\quad - \sqrt{\frac{1}{2}}\hat{x}_{\text{an3}}^{(0)}e^{r_3}, \\
 \hat{p}_3 &= \frac{1}{3}\hat{p}_{\text{in}} + \frac{\sqrt{2}}{3}\hat{p}_{\text{an1}}^{(0)}e^{r_1} - \sqrt{\frac{1}{6}}\hat{p}_{\text{an2}}^{(0)}e^{-r_2} \\
 &\quad - \sqrt{\frac{1}{2}}\hat{p}_{\text{an3}}^{(0)}e^{-r_3}, \\
 \hat{x}_4 &= \frac{1}{3}\hat{x}_{\text{in}} - \frac{1}{3\sqrt{2}}\hat{x}_{\text{an1}}^{(0)}e^{-r_1} + \sqrt{\frac{1}{6}}\hat{x}_{\text{an4}}^{(0)}e^{-r_4} \\
 &\quad + \sqrt{\frac{2}{3}}\hat{x}_{\text{an5}}^{(0)}e^{r_5}, \\
 \hat{p}_4 &= \frac{1}{3}\hat{p}_{\text{in}} - \frac{1}{3\sqrt{2}}\hat{p}_{\text{an1}}^{(0)}e^{r_1} + \sqrt{\frac{1}{6}}\hat{p}_{\text{an4}}^{(0)}e^{r_4} \\
 &\quad + \sqrt{\frac{2}{3}}\hat{p}_{\text{an5}}^{(0)}e^{-r_5}, \\
 \hat{x}_5 &= \frac{1}{3}\hat{x}_{\text{in}} - \frac{1}{3\sqrt{2}}\hat{x}_{\text{an1}}^{(0)}e^{-r_1} + \sqrt{\frac{1}{6}}\hat{x}_{\text{an4}}^{(0)}e^{-r_4} \\
 &\quad - \sqrt{\frac{1}{6}}\hat{x}_{\text{an5}}^{(0)}e^{r_5} + \sqrt{\frac{1}{2}}\hat{x}_{\text{an6}}^{(0)}e^{r_6}, \\
 \hat{p}_5 &= \frac{1}{3}\hat{p}_{\text{in}} - \frac{1}{3\sqrt{2}}\hat{p}_{\text{an1}}^{(0)}e^{r_1} + \sqrt{\frac{1}{6}}\hat{p}_{\text{an4}}^{(0)}e^{r_4} \\
 &\quad - \sqrt{\frac{1}{6}}\hat{p}_{\text{an5}}^{(0)}e^{-r_5} + \sqrt{\frac{1}{2}}\hat{p}_{\text{an6}}^{(0)}e^{-r_6}, \\
 \hat{x}_6 &= \frac{1}{3}\hat{x}_{\text{in}} - \frac{1}{3\sqrt{2}}\hat{x}_{\text{an1}}^{(0)}e^{-r_1} + \sqrt{\frac{1}{6}}\hat{x}_{\text{an4}}^{(0)}e^{-r_4}
 \end{aligned}$$

$$\begin{aligned}
& -\sqrt{\frac{1}{6}}\hat{x}_{\text{an5}}^{(0)}e^{r_5} - \sqrt{\frac{1}{2}}\hat{x}_{\text{an6}}^{(0)}e^{r_6}, \\
\hat{p}_6 &= \frac{1}{3}\hat{p}_{\text{in}} - \frac{1}{3\sqrt{2}}\hat{p}_{\text{an1}}^{(0)}e^{r_1} + \sqrt{\frac{1}{6}}\hat{p}_{\text{an4}}^{(0)}e^{r_4} \\
& -\sqrt{\frac{1}{6}}\hat{p}_{\text{an5}}^{(0)}e^{-r_5} - \sqrt{\frac{1}{2}}\hat{p}_{\text{an6}}^{(0)}e^{-r_6}, \\
\hat{x}_7 &= \frac{1}{3}\hat{x}_{\text{in}} - \frac{1}{3\sqrt{2}}\hat{x}_{\text{an1}}^{(0)}e^{-r_1} \\
& -\sqrt{\frac{1}{6}}\hat{x}_{\text{an4}}^{(0)}e^{-r_4} + \sqrt{\frac{2}{3}}\hat{x}_{\text{an7}}^{(0)}e^{r_7}, \\
\hat{p}_7 &= \frac{1}{3}\hat{p}_{\text{in}} - \frac{1}{3\sqrt{2}}\hat{p}_{\text{an1}}^{(0)}e^{r_1} - \sqrt{\frac{1}{6}}\hat{p}_{\text{an4}}^{(0)}e^{r_4} \\
& + \sqrt{\frac{2}{3}}\hat{p}_{\text{an7}}^{(0)}e^{-r_7}, \\
\hat{x}_8 &= \frac{1}{3}\hat{x}_{\text{in}} - \frac{1}{3\sqrt{2}}\hat{x}_{\text{an1}}^{(0)}e^{-r_1} - \sqrt{\frac{1}{6}}\hat{x}_{\text{an4}}^{(0)}e^{-r_4} \\
& -\sqrt{\frac{1}{6}}\hat{x}_{\text{an7}}^{(0)}e^{r_7} + \sqrt{\frac{1}{2}}\hat{x}_{\text{an8}}^{(0)}e^{r_8}, \\
\hat{p}_8 &= \frac{1}{3}\hat{p}_{\text{in}} - \frac{1}{3\sqrt{2}}\hat{p}_{\text{an1}}^{(0)}e^{r_1} - \sqrt{\frac{1}{6}}\hat{p}_{\text{an4}}^{(0)}e^{r_4} \\
& -\sqrt{\frac{1}{6}}\hat{p}_{\text{an7}}^{(0)}e^{-r_7} + \sqrt{\frac{1}{2}}\hat{p}_{\text{an8}}^{(0)}e^{-r_8}, \\
\hat{x}_9 &= \frac{1}{3}\hat{x}_{\text{in}} - \frac{1}{3\sqrt{2}}\hat{x}_{\text{an1}}^{(0)}e^{-r_1} - \sqrt{\frac{1}{6}}\hat{x}_{\text{an4}}^{(0)}e^{-r_4} \\
& -\sqrt{\frac{1}{6}}\hat{x}_{\text{an7}}^{(0)}e^{r_7} - \sqrt{\frac{1}{2}}\hat{x}_{\text{an8}}^{(0)}e^{r_8}, \\
\hat{p}_9 &= \frac{1}{3}\hat{p}_{\text{in}} - \frac{1}{3\sqrt{2}}\hat{p}_{\text{an1}}^{(0)}e^{r_1} - \sqrt{\frac{1}{6}}\hat{p}_{\text{an4}}^{(0)}e^{r_4} \\
& -\sqrt{\frac{1}{6}}\hat{p}_{\text{an7}}^{(0)}e^{-r_7} - \sqrt{\frac{1}{2}}\hat{p}_{\text{an8}}^{(0)}e^{-r_8}. \tag{A1}
\end{aligned}$$

Note that with respect to these subscripts, eq. (3) can be expressed by  $T_{789}T_{456}T_{123}T_{147}$  for modes 1 (signal input), 2 (“an2”), 3 (“an3”), 4 (“an1”), 5 (“an5”), 6 (“an6”), 7 (“an4”), 8 (“an7”), and 9 (“an8”).

The encoded state exhibits the following quadrature quantum correlations in the case of nonzero squeezing,

$$\begin{aligned}
& \hat{x}_1 + \hat{x}_2 + \hat{x}_3 - (\hat{x}_4 + \hat{x}_5 + \hat{x}_6) \\
&= \frac{3}{\sqrt{2}}\hat{x}_{\text{an1}}^{(0)}e^{-r_1} - \sqrt{\frac{3}{2}}\hat{x}_{\text{an4}}^{(0)}e^{-r_4}, \\
& \hat{x}_4 + \hat{x}_5 + \hat{x}_6 - (\hat{x}_7 + \hat{x}_8 + \hat{x}_9) \\
&= \sqrt{6}\hat{x}_{\text{an4}}^{(0)}e^{-r_4}, \\
& \hat{p}_1 - \hat{p}_2 = \sqrt{\frac{3}{2}}\hat{p}_{\text{an2}}^{(0)}e^{-r_2} - \frac{1}{\sqrt{2}}\hat{p}_{\text{an3}}^{(0)}e^{-r_3}, \\
& \hat{p}_2 - \hat{p}_3 = \sqrt{2}\hat{p}_{\text{an3}}^{(0)}e^{-r_3}, \\
& \hat{p}_4 - \hat{p}_5 = \sqrt{\frac{3}{2}}\hat{p}_{\text{an5}}^{(0)}e^{-r_5} - \frac{1}{\sqrt{2}}\hat{p}_{\text{an6}}^{(0)}e^{-r_6}, \\
& \hat{p}_5 - \hat{p}_6 = \sqrt{2}\hat{p}_{\text{an6}}^{(0)}e^{-r_6},
\end{aligned}$$

$$\begin{aligned}
\hat{p}_7 - \hat{p}_8 &= \sqrt{\frac{3}{2}}\hat{p}_{\text{an7}}^{(0)}e^{-r_7} - \frac{1}{\sqrt{2}}\hat{p}_{\text{an8}}^{(0)}e^{-r_8}, \\
\hat{p}_8 - \hat{p}_9 &= \sqrt{2}\hat{p}_{\text{an8}}^{(0)}e^{-r_8}. \tag{A2}
\end{aligned}$$

In the limit  $r_{1-8} \rightarrow \infty$ , the quadrature operators become perfectly correlated,

$$\begin{aligned}
\hat{x}_1 + \hat{x}_2 + \hat{x}_3 &= \hat{x}_4 + \hat{x}_5 + \hat{x}_6 = \hat{x}_7 + \hat{x}_8 + \hat{x}_9, \\
\hat{p}_1 &= \hat{p}_2 = \hat{p}_3, \\
\hat{p}_4 &= \hat{p}_5 = \hat{p}_6, \\
\hat{p}_7 &= \hat{p}_8 = \hat{p}_9. \tag{A3}
\end{aligned}$$

These correlations are analogous expressions to the eight stabilizer conditions of the Shor qubit code (where for continuous variables, Pauli operators are replaced by Weyl-Heisenberg phase-space operators). Note that these correlations hold for *any* signal input state, i.e., for any resulting “code words”, again similar to the stabilizer conditions for qubits. In order to obtain a sufficient set of entanglement witnesses for verifying a fully inseparable nine-party state, additional quadrature correlations must be considered; these extra correlations are expressed in terms of the “logical” quadratures in the code space which depend also on the signal state (see appendix E).

## APPENDIX B: DECODING AND CORRECTION

Random phase fluctuations are transferred onto one selected beam of the encoded state, leading to random phase-space displacements of one of the nine optical modes. This effect can be described by adding error quadrature operators to the corresponding mode  $k$ ,  $\lambda_k \hat{x}_k^e$  and  $\lambda_k \hat{p}_k^e$ , where the parameter  $\lambda_k$  will be set to one for the single mode of the noisy quantum channel and otherwise chosen to be zero. After the decoding step,  $T_{147}^{-1}T_{123}^{-1}T_{456}^{-1}T_{789}^{-1}$ , the outgoing quadrature operators become

$$\begin{aligned}
\hat{x}'_1 &= \hat{x}_{\text{in}} + \frac{1}{3} \sum_{k=1}^9 \lambda_k \hat{x}_k^e, \\
\hat{p}'_1 &= \hat{p}_{\text{in}} + \frac{1}{3} \sum_{k=1}^9 \lambda_k \hat{p}_k^e, \\
\hat{x}'_2 &= \hat{x}_{\text{an2}}^{(0)}e^{r_2} + \sqrt{\frac{2}{3}}\lambda_1 \hat{x}_1^e - \frac{1}{\sqrt{6}}(\lambda_2 \hat{x}_2^e + \lambda_3 \hat{x}_3^e), \\
\hat{p}'_2 &= \hat{p}_{\text{an2}}^{(0)}e^{-r_2} + \sqrt{\frac{2}{3}}\lambda_1 \hat{p}_1^e - \frac{1}{\sqrt{6}}(\lambda_2 \hat{p}_2^e + \lambda_3 \hat{p}_3^e), \\
\hat{x}'_3 &= \hat{x}_{\text{an3}}^{(0)}e^{r_3} + \frac{1}{\sqrt{2}}(\lambda_2 \hat{x}_2^e - \lambda_3 \hat{x}_3^e), \\
\hat{p}'_3 &= \hat{p}_{\text{an3}}^{(0)}e^{-r_3} + \frac{1}{\sqrt{2}}(\lambda_2 \hat{p}_2^e - \lambda_3 \hat{p}_3^e),
\end{aligned}$$

$$\begin{aligned}
\hat{x}'_4 &= \hat{x}_{\text{an1}}^{(0)} e^{-r_1} + \frac{\sqrt{2}}{3} \sum_{k=1}^3 \lambda_k \hat{x}_k^e - \frac{1}{\sqrt{18}} \sum_{k=4}^9 \lambda_k \hat{x}_k^e, \\
\hat{p}'_4 &= \hat{p}_{\text{an1}}^{(0)} e^{r_1} + \frac{\sqrt{2}}{3} \sum_{k=1}^3 \lambda_k \hat{p}_k^e - \frac{1}{\sqrt{18}} \sum_{k=4}^9 \lambda_k \hat{p}_k^e, \\
\hat{x}'_5 &= \hat{x}_{\text{an5}}^{(0)} e^{r_5} + \sqrt{\frac{2}{3}} \lambda_4 \hat{x}_4^e - \frac{1}{\sqrt{6}} (\lambda_5 \hat{x}_5^e + \lambda_6 \hat{x}_6^e), \\
\hat{p}'_5 &= \hat{p}_{\text{an5}}^{(0)} e^{-r_5} + \sqrt{\frac{2}{3}} \lambda_4 \hat{p}_4^e - \frac{1}{\sqrt{6}} (\lambda_5 \hat{p}_5^e + \lambda_6 \hat{p}_6^e), \\
\hat{x}'_6 &= \hat{x}_{\text{an6}}^{(0)} e^{r_6} + \frac{1}{\sqrt{2}} (\lambda_5 \hat{x}_5^e - \lambda_6 \hat{x}_6^e), \\
\hat{p}'_6 &= \hat{p}_{\text{an6}}^{(0)} e^{-r_6} + \frac{1}{\sqrt{2}} (\lambda_5 \hat{p}_5^e - \lambda_6 \hat{p}_6^e), \\
\hat{x}'_7 &= \hat{x}_{\text{an4}}^{(0)} e^{-r_4} + \frac{1}{\sqrt{6}} \left( \sum_{k=4}^6 \lambda_k \hat{x}_k^e - \sum_{k=7}^9 \lambda_k \hat{x}_k^e \right), \\
\hat{p}'_7 &= \hat{p}_{\text{an4}}^{(0)} e^{r_4} + \frac{1}{\sqrt{6}} \left( \sum_{k=4}^6 \lambda_k \hat{p}_k^e - \sum_{k=7}^9 \lambda_k \hat{p}_k^e \right), \\
\hat{x}'_8 &= \hat{x}_{\text{an7}}^{(0)} e^{r_7} + \sqrt{\frac{2}{3}} \lambda_7 \hat{x}_7^e - \frac{1}{\sqrt{6}} (\lambda_8 \hat{x}_8^e + \lambda_9 \hat{x}_9^e), \\
\hat{p}'_8 &= \hat{p}_{\text{an7}}^{(0)} e^{-r_7} + \sqrt{\frac{2}{3}} \lambda_7 \hat{p}_7^e - \frac{1}{\sqrt{6}} (\lambda_8 \hat{p}_8^e + \lambda_9 \hat{p}_9^e), \\
\hat{x}'_9 &= \hat{x}_{\text{an8}}^{(0)} e^{r_8} + \frac{1}{\sqrt{2}} (\lambda_8 \hat{x}_8^e - \lambda_9 \hat{x}_9^e), \\
\hat{p}'_9 &= \hat{p}_{\text{an8}}^{(0)} e^{-r_8} + \frac{1}{\sqrt{2}} (\lambda_8 \hat{p}_8^e - \lambda_9 \hat{p}_9^e).
\end{aligned} \tag{B1}$$

Modes two through nine are measured via suitable homodyne detectors, i.e., the local oscillator phase is adjusted to detect those quadratures which are quiet if there was no error. After the corresponding feedforward operations on the first mode, the signal input state will be recovered in mode 1 up to the finite squeezing from the ancilla modes.

For example, in the case of an error transferred onto mode 1,  $\lambda_k = \delta_{k1}$ ,

$$\begin{aligned}
\hat{x}'_1 &= \hat{x}_{\text{in}} + \frac{1}{3} \hat{x}_1^e, \\
\hat{p}'_1 &= \hat{p}_{\text{in}} + \frac{1}{3} \hat{p}_1^e,
\end{aligned} \tag{B2}$$

only for detectors 1 and 2 (see Fig. 2 of main body), measuring  $\hat{x}'_4$  (position of “an1”) and  $\hat{p}'_2$  (momentum of “an2”), respectively, results clearly different from zero (coming from the error) are obtained. All the remaining detectors show results around zero. In order to correct the error, mode 1 is displaced according to

$$\begin{aligned}
\hat{x}'_1 &\rightarrow \hat{x}'_1 - \frac{1}{\sqrt{2}} \hat{x}'_4, \\
\hat{p}'_1 &\rightarrow \hat{p}'_1 - \frac{1}{\sqrt{6}} \hat{p}'_2,
\end{aligned} \tag{B3}$$

leading to

$$\begin{aligned}
\hat{x}_{\text{out}} &= \hat{x}_{\text{in}} - \frac{1}{\sqrt{2}} \hat{x}_{\text{an1}}^{(0)} e^{-r_1}, \\
\hat{p}_{\text{out}} &= \hat{p}_{\text{in}} - \frac{1}{\sqrt{6}} \hat{p}_{\text{an2}}^{(0)} e^{-r_2},
\end{aligned} \tag{B4}$$

using eqs. (B1).

Similarly, in the case of an error transferred onto mode 9,  $\lambda_k = \delta_{k9}$ , we have

$$\begin{aligned}
\hat{x}'_1 &= \hat{x}_{\text{in}} + \frac{1}{3} \hat{x}_9^e, \\
\hat{p}'_1 &= \hat{p}_{\text{in}} + \frac{1}{3} \hat{p}_9^e.
\end{aligned} \tag{B5}$$

Now the only nonzero outputs occur at detectors 1 and 4 (Fig. 2), measuring  $\hat{x}'_4$  (position of “an1”) and  $\hat{x}'_7$  (position of “an4”), respectively, and at detectors 7 and 8, measuring  $\hat{p}'_8$  (momentum of “an7”) and  $\hat{p}'_9$  (momentum of “an8”), respectively. Possible correction displacements are

$$\begin{aligned}
\hat{x}'_1 &\rightarrow \hat{x}'_1 + \sqrt{2} \hat{x}'_4, \\
\hat{x}'_1 &\rightarrow \hat{x}'_1 + \sqrt{\frac{2}{3}} \hat{x}'_7,
\end{aligned} \tag{B6}$$

for  $x$ , and

$$\begin{aligned}
\hat{p}'_1 &\rightarrow \hat{p}'_1 + \sqrt{\frac{2}{3}} \hat{p}'_8, \\
\hat{p}'_1 &\rightarrow \hat{p}'_1 + \frac{\sqrt{2}}{3} \hat{p}'_9,
\end{aligned} \tag{B7}$$

for  $p$ . These corrections result in the output quadratures

$$\begin{aligned}
\hat{x}_{\text{out}} &= \hat{x}_{\text{in}} + \sqrt{2} \hat{x}_{\text{an1}}^{(0)} e^{-r_1}, \\
\hat{x}_{\text{out}} &= \hat{x}_{\text{in}} + \sqrt{\frac{2}{3}} \hat{x}_{\text{an4}}^{(0)} e^{-r_4}, \\
\hat{p}_{\text{out}} &= \hat{p}_{\text{in}} + \sqrt{\frac{2}{3}} \hat{p}_{\text{an7}}^{(0)} e^{-r_7}, \\
\hat{p}_{\text{out}} &= \hat{p}_{\text{in}} + \frac{\sqrt{2}}{3} \hat{p}_{\text{an8}}^{(0)} e^{-r_8},
\end{aligned} \tag{B8}$$

always nearly recovering the signal input state.

Similar calculations yield the quadrature operators for the output state of mode 1 after the error correction protocol in the case of an error on modes two through eight; for an error on mode 2,

$$\begin{aligned}
\hat{x}_{\text{out,det1}} &= \hat{x}_{\text{in}} - \frac{1}{\sqrt{2}} \hat{x}_{\text{an1}}^{(0)} e^{-r_1}, \\
\hat{p}_{\text{out,det2}} &= \hat{p}_{\text{in}} + \sqrt{\frac{2}{3}} \hat{p}_{\text{an2}}^{(0)} e^{-r_2}, \\
\hat{p}_{\text{out,det3}} &= \hat{p}_{\text{in}} - \frac{\sqrt{2}}{3} \hat{p}_{\text{an3}}^{(0)} e^{-r_3},
\end{aligned} \tag{B9}$$

for an error on mode 3,

$$\begin{aligned}\hat{x}_{\text{out,det1}} &= \hat{x}_{\text{in}} - \frac{1}{\sqrt{2}}\hat{x}_{\text{an1}}^{(0)}e^{-r_1}, \\ \hat{p}_{\text{out,det2}} &= \hat{p}_{\text{in}} + \sqrt{\frac{2}{3}}\hat{p}_{\text{an2}}^{(0)}e^{-r_2}, \\ \hat{p}_{\text{out,det3}} &= \hat{p}_{\text{in}} + \frac{\sqrt{2}}{3}\hat{p}_{\text{an3}}^{(0)}e^{-r_3},\end{aligned}\quad (\text{B10})$$

for an error on mode 4,

$$\begin{aligned}\hat{x}_{\text{out,det1}} &= \hat{x}_{\text{in}} + \sqrt{2}\hat{x}_{\text{an1}}^{(0)}e^{-r_1}, \\ \hat{x}_{\text{out,det4}} &= \hat{x}_{\text{in}} - \sqrt{\frac{2}{3}}\hat{x}_{\text{an4}}^{(0)}e^{-r_4}, \\ \hat{p}_{\text{out,det5}} &= \hat{p}_{\text{in}} - \frac{1}{\sqrt{6}}\hat{p}_{\text{an5}}^{(0)}e^{-r_5},\end{aligned}\quad (\text{B11})$$

for an error on mode 5,

$$\begin{aligned}\hat{x}_{\text{out,det1}} &= \hat{x}_{\text{in}} + \sqrt{2}\hat{x}_{\text{an1}}^{(0)}e^{-r_1}, \\ \hat{x}_{\text{out,det4}} &= \hat{x}_{\text{in}} - \sqrt{\frac{2}{3}}\hat{x}_{\text{an4}}^{(0)}e^{-r_4}, \\ \hat{p}_{\text{out,det5}} &= \hat{p}_{\text{in}} - \sqrt{\frac{2}{3}}\hat{p}_{\text{an5}}^{(0)}e^{-r_5}, \\ \hat{p}_{\text{out,det6}} &= \hat{p}_{\text{in}} - \frac{\sqrt{2}}{3}\hat{p}_{\text{an6}}^{(0)}e^{-r_6},\end{aligned}\quad (\text{B12})$$

for an error on mode 6,

$$\begin{aligned}\hat{x}_{\text{out,det1}} &= \hat{x}_{\text{in}} + \sqrt{2}\hat{x}_{\text{an1}}^{(0)}e^{-r_1}, \\ \hat{x}_{\text{out,det4}} &= \hat{x}_{\text{in}} - \sqrt{\frac{2}{3}}\hat{x}_{\text{an4}}^{(0)}e^{-r_4}, \\ \hat{p}_{\text{out,det5}} &= \hat{p}_{\text{in}} + \sqrt{\frac{2}{3}}\hat{p}_{\text{an5}}^{(0)}e^{-r_5}, \\ \hat{p}_{\text{out,det6}} &= \hat{p}_{\text{in}} + \frac{\sqrt{2}}{3}\hat{p}_{\text{an6}}^{(0)}e^{-r_6},\end{aligned}\quad (\text{B13})$$

for an error on mode 7,

$$\begin{aligned}\hat{x}_{\text{out,det1}} &= \hat{x}_{\text{in}} + \sqrt{2}\hat{x}_{\text{an1}}^{(0)}e^{-r_1}, \\ \hat{x}_{\text{out,det4}} &= \hat{x}_{\text{in}} + \sqrt{\frac{2}{3}}\hat{x}_{\text{an4}}^{(0)}e^{-r_4}, \\ \hat{p}_{\text{out,det7}} &= \hat{p}_{\text{in}} - \frac{1}{\sqrt{6}}\hat{p}_{\text{an7}}^{(0)}e^{-r_7},\end{aligned}\quad (\text{B14})$$

for an error on mode 8,

$$\begin{aligned}\hat{x}_{\text{out,det1}} &= \hat{x}_{\text{in}} + \sqrt{2}\hat{x}_{\text{an1}}^{(0)}e^{-r_1}, \\ \hat{x}_{\text{out,det4}} &= \hat{x}_{\text{in}} + \sqrt{\frac{2}{3}}\hat{x}_{\text{an4}}^{(0)}e^{-r_4}, \\ \hat{p}_{\text{out,det7}} &= \hat{p}_{\text{in}} + \sqrt{\frac{2}{3}}\hat{p}_{\text{an7}}^{(0)}e^{-r_7}, \\ \hat{p}_{\text{out,det8}} &= \hat{p}_{\text{in}} - \frac{\sqrt{2}}{3}\hat{p}_{\text{an8}}^{(0)}e^{-r_8}.\end{aligned}\quad (\text{B15})$$

The additional subscripts ‘‘det1’’, etc., indicate which detector outcomes are used for the correction displacements. These detectors (see Fig. 2) measure the quadratures  $\hat{x}'_4$  (‘‘det1’’),  $\hat{p}'_2$  (‘‘det2’’),  $\hat{p}'_3$  (‘‘det3’’),  $\hat{x}'_7$  (‘‘det4’’),  $\hat{p}'_5$  (‘‘det5’’),  $\hat{p}'_6$  (‘‘det6’’),  $\hat{p}'_8$  (‘‘det7’’), and  $\hat{p}'_9$  (‘‘det8’’).

Because of the freedom in choosing the correction displacements, there is always an optimal feedforward operation. For example, in the case of an error on mode 2,

$$\begin{aligned}\hat{x}_{\text{out}} &= \hat{x}_{\text{in}} - \frac{1}{\sqrt{2}}\hat{x}_{\text{an1}}^{(0)}e^{-r_1}, \\ \hat{p}_{\text{out,det2}} &= \hat{p}_{\text{in}} + \sqrt{\frac{2}{3}}\hat{p}_{\text{an2}}^{(0)}e^{-r_2}, \\ \hat{p}_{\text{out,det3}} &= \hat{p}_{\text{in}} - \frac{\sqrt{2}}{3}\hat{p}_{\text{an3}}^{(0)}e^{-r_3},\end{aligned}\quad (\text{B16})$$

we obtain the following excess noise for the output state,

$$\begin{aligned}\langle(\hat{x}_{\text{out}})^2\rangle &= \langle(\hat{x}_{\text{in}})^2\rangle + \frac{1}{2} \cdot \frac{1}{4}e^{-2r_1}, \\ \langle(\hat{p}_{\text{out,det2}})^2\rangle &= \langle(\hat{p}_{\text{in}})^2\rangle + \frac{2}{3} \cdot \frac{1}{4}e^{-2r_2}, \\ \langle(\hat{p}_{\text{out,det3}})^2\rangle &= \langle(\hat{p}_{\text{in}})^2\rangle + \frac{2}{9} \cdot \frac{1}{4}e^{-2r_3}.\end{aligned}\quad (\text{B17})$$

However, for  $r_2 = r_3 = r$ , the optimal feedforward operation leads to

$$\hat{p}_{\text{out,opt}} = \hat{p}_{\text{in}} + \frac{1}{2\sqrt{6}}\hat{p}_{\text{an2}}^{(0)}e^{-r} - \frac{\sqrt{2}}{4}\hat{p}_{\text{an3}}^{(0)}e^{-r},\quad (\text{B18})$$

corresponding to

$$\langle(\hat{p}_{\text{out,opt}})^2\rangle = \langle(\hat{p}_{\text{in}})^2\rangle + \frac{1}{6} \cdot \frac{1}{4}e^{-2r},\quad (\text{B19})$$

which is the same as for the case of an error on mode 1. For unequal squeezing,  $r_2 \neq r_3$ , the optimal feedforward depends on the squeezing values. Therefore, in the current experiment, we use only the output of detector 3 for the feedforward. Table B shows which outputs of the homodyne detectors are used for error correction.

### APPENDIX C: RESULTS OF ERROR SYNDROME MEASUREMENTS

Fig. 5 shows error syndrome measurement results. Here, the input state is a vacuum state. This case is also described in the main body of the paper. A random displacement error in phase space is transferred onto quantum channels one through nine for A-I, respectively. With Table 1 in the main body of the paper and Fig. 5 here, we can decide which quantum channel is subject to an error and derive a corresponding feedforward operation to correct the error.



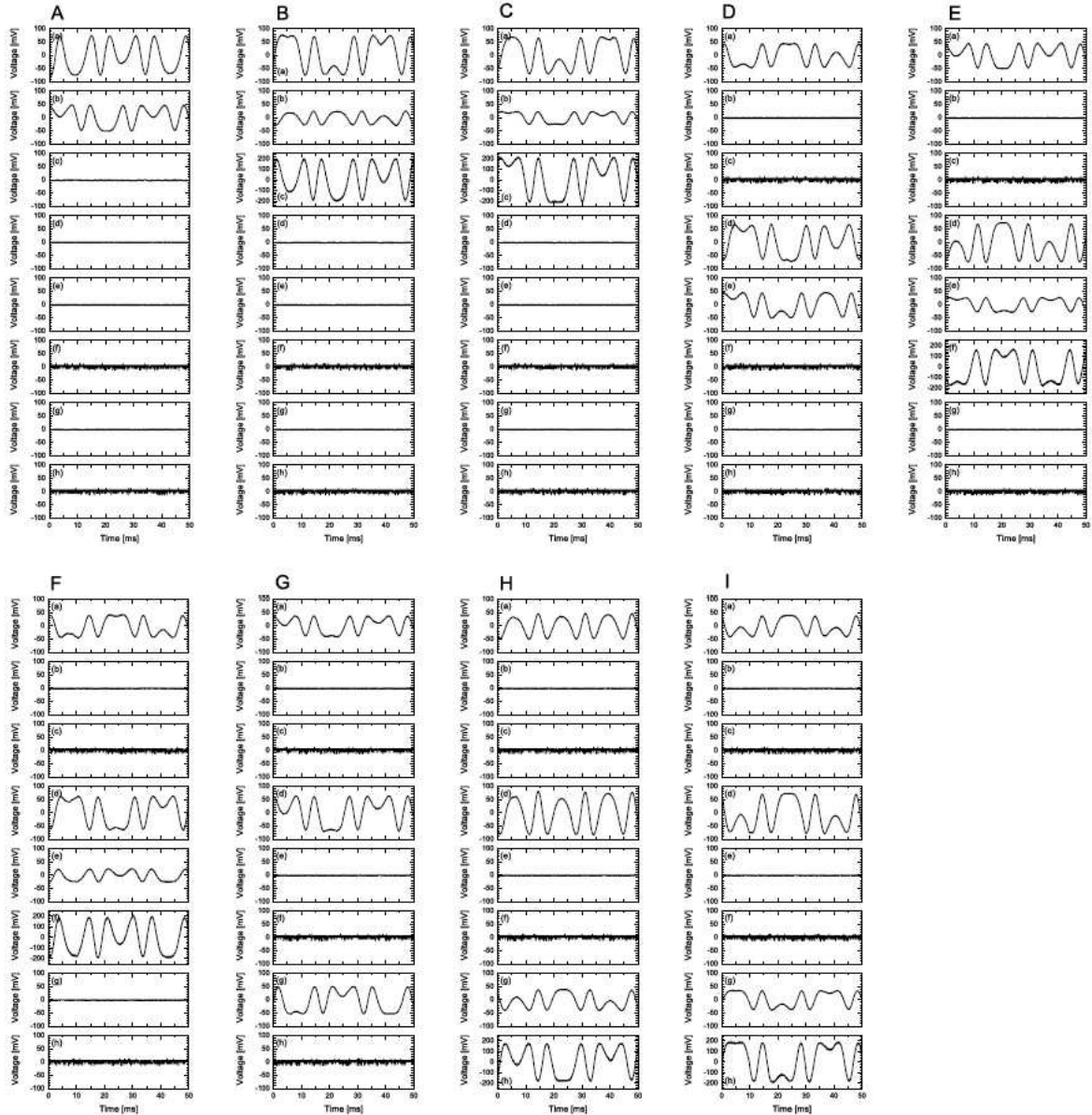


FIG. 5: Results of error syndrome measurements. A-I correspond to the cases of an error in quantum channels 1-9, respectively. (a)-(h) correspond to outputs from homodyne detectors 1-8, respectively.

#### APPENDIX D: RESULTS OF ERROR CORRECTION

Fig. 6 shows the results of error correction. The results are summarized in Table 2 in the main body of the paper.

#### APPENDIX E: THE ROLE OF MULTIPARTITE ENTANGLEMENT

The encoded nine-mode state, as created in the current experiment and described by eqs. (A1), approaches the

following state in the limit of infinite squeezing,

$$|\psi_{\text{encode}}\rangle = \frac{1}{\pi^{3/2}} \int dp \, dp_1 \, dp_2 \, dp_3 \, \bar{\psi}(p) e^{-2ip(p_1+p_2+p_3)} \times |p_1, p_1, p_1, p_2, p_2, p_2, p_3, p_3, p_3\rangle. \quad (\text{E1})$$

Clearly, even for infinite squeezing and perfect encoding, the inseparability properties of the total nine-party state depend on the signal input wave function  $\bar{\psi}(p)$ . In particular, for  $\bar{\psi}(p) \equiv \delta(p)$ , we obtain  $|\psi_{\text{encode}}\rangle = \int dp |p, p, p\rangle \otimes \int dp |p, p, p\rangle \otimes \int dp |p, p, p\rangle$ , which is clearly not fully nine-party entangled, but rather a product state of three fully tripartite entangled GHZ-type three-mode states. So in order to obtain full nine-party entangle-

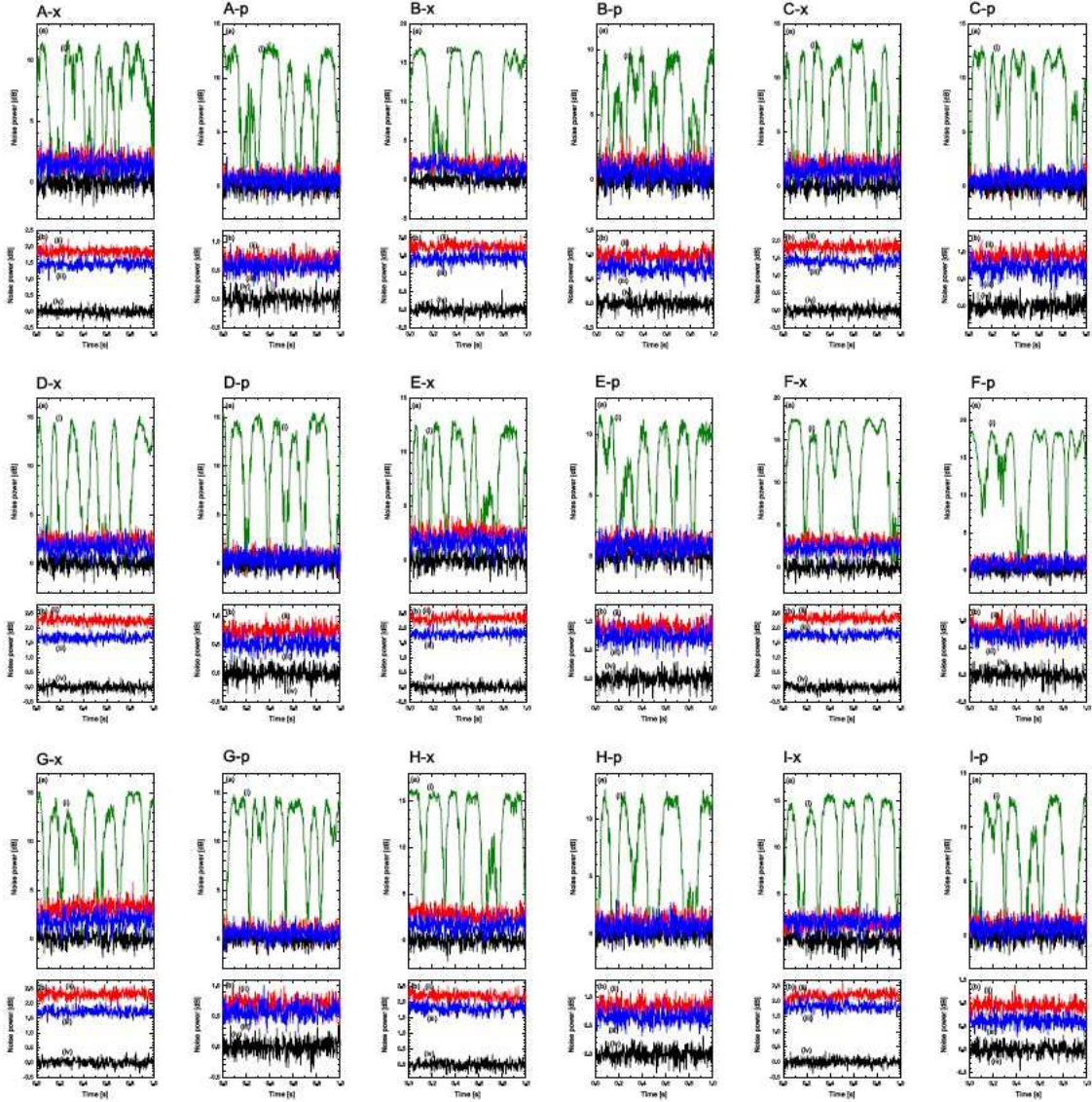


FIG. 6: Results of error correction. A-I correspond to the cases of an error in quantum channels 1-9, respectively. The LO phase of the homodyne detector is locked at  $x$  or  $p$ , which is indicated after the capital letters. Trace numbers are the same as in Figs. (5) and (6) in the main body of the paper.

ment, the input state should not correspond to an infinitely  $x$ -squeezed state (corresponding, after Fourier transform, to  $\bar{\psi}(p) \equiv \delta(p)$ ). Similarly, an infinitely  $p$ -squeezed input state leads to vanishing GHZ-type correlations *within* each of the three triplets, but it has excellent GHZ-type correlations *between* the three triplets. For an input state between these two extremes, for instance, a vacuum input state as used in the experiment, we obtain quadrature correlations of both types, potentially leading to full nine-party entanglement.

In order to witness full nine-party entanglement, in addition to the correlations of eqs. (A3),  $p$ -correlations *between* the triplets and  $x$ -correlations *within* each triplet are required. Equations (A3) only describe  $x$ -correlations between the triplets and  $p$ -correlations within each

triplet. The missing correlations are of the type of  $\hat{p}_1 + \hat{p}_4 + \hat{p}_7 \rightarrow 0$  and  $\hat{x}_1 + \hat{x}_2 + \hat{x}_3 \rightarrow 0$ . These linear combinations correspond to the “logical” quadratures in the code space,

$$\begin{aligned} \hat{X} &\equiv \hat{x}_1 + \hat{x}_2 + \hat{x}_3 = \hat{x}_{\text{in}} + \sqrt{2}\hat{x}_{\text{an1}}^{(0)} e^{-r_1}, \\ \hat{P} &\equiv \hat{p}_1 + \hat{p}_4 + \hat{p}_7 = \hat{p}_{\text{in}} + \sqrt{\frac{2}{3}}\hat{p}_{\text{an2}}^{(0)} e^{-r_2} \\ &\quad + \sqrt{\frac{2}{3}}\hat{p}_{\text{an5}}^{(0)} e^{-r_5} + \sqrt{\frac{2}{3}}\hat{p}_{\text{an7}}^{(0)} e^{-r_7}, \end{aligned} \quad (\text{E2})$$

obviously depending on the signal input state. Only for infinite ancilla squeezing, the encoding is perfect,  $\hat{X} = \hat{x}_{\text{in}}$  and  $\hat{P} = \hat{p}_{\text{in}}$ . The excess noise in each quadrature is  $2 \times e^{-2r}/4$  for equal squeezing of the ancilla

TABLE III: Homodyne detector outputs for feedforward in the current experiments.

channel with an error	quadrature	detectors for feedforward
1	$x$	1
	$p$	2
2	$x$	1
	$p$	3
3	$x$	1
	$p$	3
4	$x$	4
	$p$	5
5	$x$	4
	$p$	6
6	$x$	4
	$p$	6
7	$x$	4
	$p$	7
8	$x$	4
	$p$	8
9	$x$	4
	$p$	8

modes. In this case, an infinitely  $x$ -squeezed input state would lead to excellent intra-triplet  $x$ -correlations; an infinitely  $p$ -squeezed input state, favorable for good inter-triplet  $p$ -correlations, leads to vanishing intra-triplet  $x$ -correlations. With a vacuum input state, as used in the experiment, we have both types of quantum correlations for nonzero squeezing of the ancilla modes. Similar quantum correlations also exist for the combinations

$$\begin{aligned}
\hat{x}_4 + \hat{x}_5 + \hat{x}_6 &= \hat{x}_{\text{in}} - \frac{1}{\sqrt{2}} \hat{x}_{\text{an1}}^{(0)} e^{-r_1} + \sqrt{\frac{3}{2}} \hat{x}_{\text{an4}}^{(0)} e^{-r_4}, \\
\hat{x}_7 + \hat{x}_8 + \hat{x}_9 &= \hat{x}_{\text{in}} - \frac{1}{\sqrt{2}} \hat{x}_{\text{an1}}^{(0)} e^{-r_1} - \sqrt{\frac{3}{2}} \hat{x}_{\text{an4}}^{(0)} e^{-r_4}, \\
\hat{p}_2 + \hat{p}_5 + \hat{p}_8 &= \hat{p}_{\text{in}} - \frac{1}{\sqrt{6}} \hat{p}_{\text{an2}}^{(0)} e^{-r_2} + \sqrt{\frac{1}{2}} \hat{p}_{\text{an3}}^{(0)} e^{-r_3} \\
&\quad - \frac{1}{\sqrt{6}} \hat{p}_{\text{an5}}^{(0)} e^{-r_5} + \sqrt{\frac{1}{2}} \hat{p}_{\text{an6}}^{(0)} e^{-r_6} \\
&\quad - \frac{1}{\sqrt{6}} \hat{p}_{\text{an7}}^{(0)} e^{-r_7} + \sqrt{\frac{1}{2}} \hat{p}_{\text{an8}}^{(0)} e^{-r_8}, \\
\hat{p}_3 + \hat{p}_6 + \hat{p}_9 &= \hat{p}_{\text{in}} - \frac{1}{\sqrt{6}} \hat{p}_{\text{an2}}^{(0)} e^{-r_2} - \sqrt{\frac{1}{2}} \hat{p}_{\text{an3}}^{(0)} e^{-r_3} \\
&\quad - \frac{1}{\sqrt{6}} \hat{p}_{\text{an5}}^{(0)} e^{-r_5} - \sqrt{\frac{1}{2}} \hat{p}_{\text{an6}}^{(0)} e^{-r_6} \\
&\quad - \frac{1}{\sqrt{6}} \hat{p}_{\text{an7}}^{(0)} e^{-r_7} - \sqrt{\frac{1}{2}} \hat{p}_{\text{an8}}^{(0)} e^{-r_8}.
\end{aligned}$$

$$(E3)$$

The total set of quadrature quantum correlations can be sufficient for a fully inseparable nine-party entangled state. The corresponding nine-party entanglement witnesses lead to the known criteria for multi-party inseparability of continuous-variable states<sup>24</sup>. In order to verify three-party inseparability within each tripartite  $\hat{\rho}_{123}$ ,  $\hat{\rho}_{456}$ , and  $\hat{\rho}_{789}$ , we have, for  $\hat{\rho}_{123}$ ,

$$\begin{aligned}
\langle [\Delta(\hat{p}_1 - \hat{p}_2)]^2 \rangle + \langle [\Delta(\hat{x}_1 + \hat{x}_2 + g_{1a} \hat{x}_3)]^2 \rangle &< 1, \\
\langle [\Delta(\hat{p}_2 - \hat{p}_3)]^2 \rangle + \langle [\Delta(g_{1b} \hat{x}_1 + \hat{x}_2 + \hat{x}_3)]^2 \rangle &< 1,
\end{aligned} \tag{E4}$$

for  $\hat{\rho}_{456}$ ,

$$\begin{aligned}
\langle [\Delta(\hat{p}_4 - \hat{p}_5)]^2 \rangle + \langle [\Delta(\hat{x}_4 + \hat{x}_5 + g_{2a} \hat{x}_6)]^2 \rangle &< 1, \\
\langle [\Delta(\hat{p}_5 - \hat{p}_6)]^2 \rangle + \langle [\Delta(g_{2b} \hat{x}_4 + \hat{x}_5 + \hat{x}_6)]^2 \rangle &< 1,
\end{aligned} \tag{E5}$$

for  $\hat{\rho}_{789}$ ,

$$\begin{aligned}
\langle [\Delta(\hat{p}_7 - \hat{p}_8)]^2 \rangle + \langle [\Delta(\hat{x}_7 + \hat{x}_8 + g_{3a} \hat{x}_9)]^2 \rangle &< 1, \\
\langle [\Delta(\hat{p}_8 - \hat{p}_9)]^2 \rangle + \langle [\Delta(g_{3b} \hat{x}_7 + \hat{x}_8 + \hat{x}_9)]^2 \rangle &< 1.
\end{aligned} \tag{E6}$$

The ‘‘gains’’  $g_{1a}$ , etc., can be used to optimize these conditions. In order to rule out a state of the form  $\sum_i \eta_i \hat{\rho}_{123}^{(i)} \otimes \hat{\rho}_{456}^{(i)} \otimes \hat{\rho}_{789}^{(i)} \equiv \sum_i \eta_i \hat{\rho}_a^{(i)} \otimes \hat{\rho}_b^{(i)} \otimes \hat{\rho}_c^{(i)}$ , we need further criteria, for example,

$$\begin{aligned}
\langle [\Delta(\hat{p}_1 + \hat{p}_4 + g_{11} \hat{p}_7)]^2 \rangle & \tag{E7} \\
+ \langle [\Delta(\hat{x}_1 + g_{12} \hat{x}_2 + g_{13} \hat{x}_3 - \hat{x}_4 - g_{14} \hat{x}_5 - g_{15} \hat{x}_6)]^2 \rangle & < 1
\end{aligned}$$

$$\begin{aligned}
\langle [\Delta(g_{21} \hat{p}_1 + \hat{p}_4 + \hat{p}_7)]^2 \rangle & \tag{E8} \\
+ \langle [\Delta(\hat{x}_4 + g_{22} \hat{x}_5 + g_{23} \hat{x}_6 - \hat{x}_7 - g_{24} \hat{x}_8 - g_{25} \hat{x}_9)]^2 \rangle & < 1
\end{aligned}$$

which describe the inter-triplet correlations. Equation (E7) rules out the forms  $\sum_i \eta_i \hat{\rho}_a^{(i)} \otimes \hat{\rho}_{bc}^{(i)}$  and  $\sum_i \eta_i \hat{\rho}_b^{(i)} \otimes \hat{\rho}_{ac}^{(i)}$ ; eq. (E8) rules out the forms  $\sum_i \eta_i \hat{\rho}_c^{(i)} \otimes \hat{\rho}_{ab}^{(i)}$  and  $\sum_i \eta_i \hat{\rho}_b^{(i)} \otimes \hat{\rho}_{ac}^{(i)}$ . Thus, any form of separability between the triplets  $a$ ,  $b$ , and  $c$  can be ruled out. The inter-triplet conditions can be understood as GHZ-type correlations of modes 1, 4, and 7 after LOCC operations; namely,  $x$ -measurements of modes 2, 3, 5, 6, 8, 9 and the corresponding displacements of modes 1, 4, and 7.

In the experiment, it was verified that in any of the nine cases of an error in any one of the nine channels, the classical cutoff (zero-squeezing limit) was exceeded. This confirms that all 8 ancilla modes are in a squeezed state (see Table 1 and Fig.2), as the quadrature noise of every ancilla mode contributes to the excess noise of the corrected signal for some of the detector results used for feedforward. This squeezing translates into nonclassical correlations for all combinations in eqs. (A2), (E2), and (E3) (with a vacuum input state). The set of quadrature combinations corresponds to the ‘‘unit-gain’’ version

of the entanglement witnesses in eqs. (E4), (E5), (E6), (E7), and (E8). In order to satisfy the witness inequalities, in particular, for small squeezing values (as those of roughly 1 dB in the experiment), non-unit gain must be chosen. Although these non-unit gain combinations have not been measured directly in the quantum error correction experiment, the nonclassicality in *all* the unit-gain combinations may be interpreted as an indirect confirmation of the presence of nine-party entanglement.

## APPENDIX F: APPLICABILITY OF CONTINUOUS-VARIABLE CODES

The continuous-variable nine-mode code corrects an arbitrary error occurring in *any one* of the nine channels. Similar to the qubit case, for realistic scenarios, we should consider imperfect transmissions in *every* channel under the reasonable assumption of errors acting independently in all the channels. The performance of the code can then be evaluated by comparing the transfer fidelities for the encoded scheme with a direct transmission of the signal state through a single noisy channel<sup>12</sup>.

Using the example of a 3-wavepacket code, we shall demonstrate that for certain stochastic error models, the continuous-variable code leads to a dramatic improvement of fidelity even when the errors occur in every channel<sup>13</sup>. In this case, the errors should correspond to  $x$ -displacements or any errors decomposable into  $x$ -displacements (including non-Gaussian “ $x$ -errors”). A code for correcting arbitrary errors including non-commuting  $x$  and  $p$ -errors is obtainable, for instance, by concatenating the 3-mode code into a 9-mode code, as implemented in the current experiment. The appropriate error models are reminiscent of the most typical qubit channels such as bit-flip and phase-flip channels. In the continuous-variable regime, these types of stochastic errors would map a Gaussian signal state into a non-Gaussian state represented by a discrete, incoherent mixture of the input state with a Gaussian (or even a non-Gaussian) state,

$$W_{\text{out}}(x, p) = (1 - \gamma)W_{\text{in}} + \gamma W_{\text{error}}. \quad (\text{F1})$$

Here, the input state described by the Wigner function  $W_{\text{in}}$  is transformed into a new state  $W_{\text{error}}$  with probability  $\gamma$ ; it remains unchanged with probability  $1 - \gamma$ . A special case of the above channel model is an erasure channel<sup>19</sup>. The generalized erasure model here may find applications in free-space communication with fluctuating losses and beam point jitter effects<sup>16,17,18</sup>.

As an example, we will consider a coherent-state input,  $|\bar{\alpha}_1\rangle = |\bar{x}_1 + i\bar{p}_1\rangle$ , described by the Wigner function,

$$W_{\text{in}}(x_1, p_1) = \frac{2}{\pi} \exp[-2(x_1 - \bar{x}_1)^2 - 2(p_1 - \bar{p}_1)^2]. \quad (\text{F2})$$

Moreover, we assume that the effect of the error is just an  $x$ -displacement by  $\bar{x}_2$  such that

$$W_{\text{error}}(x_1, p_1) = W_{\text{in}}(x_1 - \bar{x}_2, p_1). \quad (\text{F3})$$

The sign of the displacement error is fixed and known, e.g., without loss of generality,  $\bar{x}_2 > 0$ . Note that more general errors, including non-Gaussian  $x$ -errors, could be considered as well.

Now in order to encode the input state, we use two ancilla modes, each in a single-mode  $x$ -squeezed vacuum state, represented by

$$W_{\text{anc}}(x_k, p_k) = \frac{2}{\pi} \exp[-2e^{+2r} x_k^2 - 2e^{-2r} p_k^2], \quad (\text{F4})$$

with squeezing parameter  $r$  and  $k = 2, 3$ . The total three-mode state before encoding is

$$W(\alpha_1, \alpha_2, \alpha_3) = W_{\text{in}}(x_1, p_1)W_{\text{anc}}(x_2, p_2)W_{\text{anc}}(x_3, p_3), \quad (\text{F5})$$

with  $\alpha_j = x_j + ip_j$ ,  $j = 1, 2, 3$ . The encoding may be achieved by applying a “tritter”, i.e., a sequence of two beam splitters with transmittances 1 : 2 and 1 : 1. The total, encoded state will be an entangled three-mode Gaussian state with Wigner function,

$$\begin{aligned} W_{\text{enc}}(\alpha_1, \alpha_2, \alpha_3) &= \left(\frac{2}{\pi}\right)^3 \quad (\text{F6}) \\ &\times \exp \left\{ -2 \left[ \frac{1}{\sqrt{3}} (x_1 + x_2 + x_3) - \bar{x}_1 \right]^2 \right. \\ &\quad - \frac{2}{3} e^{-2r} \left[ (p_1 - p_2)^2 + (p_2 - p_3)^2 + (p_1 - p_3)^2 \right] \\ &\quad - 2 \left[ \frac{1}{\sqrt{3}} (p_1 + p_2 + p_3) - \bar{p}_1 \right]^2 \\ &\quad \left. - \frac{2}{3} e^{+2r} \left[ (x_1 - x_2)^2 + (x_2 - x_3)^2 + (x_1 - x_3)^2 \right] \right\}. \end{aligned}$$

Now we send the three modes through individual channels where each channel acts independently upon *every* mode as described by Eq. (F1) with  $W_{\text{error}}$  corresponding to an  $x$ -displacement by  $\bar{x}_2$ . As a result, the three noisy channels will turn the encoded state into the following three-mode state,

$$\begin{aligned} W'_{\text{enc}}(\alpha_1, \alpha_2, \alpha_3) &\quad (\text{F7}) \\ &= (1 - \gamma)^3 W_{\text{enc}}(\alpha_1, \alpha_2, \alpha_3) \\ &\quad + \gamma(1 - \gamma)^2 W_{\text{enc}}(x_1 - \bar{x}_2 + ip_1, \alpha_2, \alpha_3) \\ &\quad + \gamma(1 - \gamma)^2 W_{\text{enc}}(\alpha_1, x_2 - \bar{x}_2 + ip_2, \alpha_3) \\ &\quad + \gamma(1 - \gamma)^2 W_{\text{enc}}(\alpha_1, \alpha_2, x_3 - \bar{x}_2 + ip_3) \\ &\quad + \gamma^2(1 - \gamma) W_{\text{enc}}(x_1 - \bar{x}_2 + ip_1, x_2 - \bar{x}_2 + ip_2, \alpha_3) \\ &\quad + \gamma^2(1 - \gamma) W_{\text{enc}}(x_1 - \bar{x}_2 + ip_1, \alpha_2, x_3 - \bar{x}_2 + ip_3) \\ &\quad + \gamma^2(1 - \gamma) W_{\text{enc}}(\alpha_1, x_2 - \bar{x}_2 + ip_2, x_3 - \bar{x}_2 + ip_3) \\ &\quad + \gamma^3 W_{\text{enc}}(x_1 - \bar{x}_2 + ip_1, x_2 - \bar{x}_2 + ip_2, x_3 - \bar{x}_2 + ip_3). \end{aligned}$$

Note that we assumed the same  $x$ -displacements in every channel.

The decoding procedure now simply means inverting

the tritter, which results in

$$\begin{aligned}
& W_{\text{dec}}(\alpha_1, \alpha_2, \alpha_3) \tag{F8} \\
&= (1 - \gamma)^3 W_{\text{in}}(x_1, p_1) W_{\text{anc}}(x_2, p_2) W_{\text{anc}}(x_3, p_3) \\
&+ \gamma(1 - \gamma)^2 W_{\text{in}}\left(x_1 - \frac{1}{\sqrt{3}}\bar{x}_2, p_1\right) \\
&\quad \times W_{\text{anc}}\left(x_2 - \sqrt{\frac{2}{3}}\bar{x}_2, p_2\right) W_{\text{anc}}(x_3, p_3) \\
&+ \gamma(1 - \gamma)^2 W_{\text{in}}\left(x_1 - \frac{1}{\sqrt{3}}\bar{x}_2, p_1\right) \\
&\quad \times W_{\text{anc}}\left(x_2 + \frac{1}{\sqrt{6}}\bar{x}_2, p_2\right) W_{\text{anc}}\left(x_3 - \frac{1}{\sqrt{2}}\bar{x}_2, p_3\right) \\
&+ \gamma(1 - \gamma)^2 W_{\text{in}}\left(x_1 - \frac{1}{\sqrt{3}}\bar{x}_2, p_1\right) \\
&\quad \times W_{\text{anc}}\left(x_2 + \frac{1}{\sqrt{6}}\bar{x}_2, p_2\right) W_{\text{anc}}\left(x_3 + \frac{1}{\sqrt{2}}\bar{x}_2, p_3\right) \\
&+ \gamma^2(1 - \gamma) W_{\text{in}}\left(x_1 - \frac{2}{\sqrt{3}}\bar{x}_2, p_1\right) \\
&\quad \times W_{\text{anc}}\left(x_2 - \frac{1}{\sqrt{6}}\bar{x}_2, p_2\right) W_{\text{anc}}\left(x_3 - \frac{1}{\sqrt{2}}\bar{x}_2, p_3\right) \\
&+ \gamma^2(1 - \gamma) W_{\text{in}}\left(x_1 - \frac{2}{\sqrt{3}}\bar{x}_2, p_1\right) \\
&\quad \times W_{\text{anc}}\left(x_2 - \frac{1}{\sqrt{6}}\bar{x}_2, p_2\right) W_{\text{anc}}\left(x_3 + \frac{1}{\sqrt{2}}\bar{x}_2, p_3\right) \\
&+ \gamma^2(1 - \gamma) W_{\text{in}}\left(x_1 - \frac{2}{\sqrt{3}}\bar{x}_2, p_1\right) \\
&\quad \times W_{\text{anc}}\left(x_2 + \sqrt{\frac{2}{3}}\bar{x}_2, p_2\right) W_{\text{anc}}(x_3, p_3) \\
&+ \gamma^3 W_{\text{in}}\left(x_1 - \sqrt{3}\bar{x}_2, p_1\right) \\
&\quad \times W_{\text{anc}}(x_2, p_2) W_{\text{anc}}(x_3, p_3).
\end{aligned}$$

By looking at this state, we can easily see that  $x$ -homodyne detections of the ancilla modes 2 and 3 (the syndrome measurements) will almost unambiguously identify in which channel a displacement error occurred and how many modes were subject to a displacement error. The only ambiguity comes from the case of an error occurring in every channel at the same time (with probability  $\gamma^3$ ), which is indistinguishable from the case where no error at all happens. In both cases, the two ancilla modes are transformed via decoding back into the two initial single-mode squeezed vacuum states. All the other cases, however, can be identified, provided the initial squeezing  $r$  is sufficiently large such that the displacements  $\propto \bar{x}_2$ , originating from the errors, can be resolved in the ancilla states.

The recovery operation, i.e., the final phase-space displacement of mode 1 depends on the syndrome measurement results for modes 2 and 3 which are consistent with either undisplaced squeezed vacuum states ('0') or squeezed vacua displaced in either '+' or '-'  $x$ -direction.

The syndrome results for modes 2 and 3 corresponding to the eight possibilities for the errors occurring in the three channels are (0,0) for no error at all, (+,0) for an error in channel 1, (-,+) for an error in channel 2, (-,-) for an error in channel 3, (+,+) for errors in channels 1 and 2, (+,-) for errors in channels 1 and 3, (-,0) for errors in channels 2 and 3, and, again, (0,0) for errors occurring in all three channels.

In the limit of infinite squeezing of the ancilla modes, the ensemble output state of mode 1 (upon averaging over all syndrome measurement results  $x_2$  and  $x_3$  including suitable feedforward operations) can be described as

$$(1 - \gamma^3)W_{\text{in}}(x_1, p_1) + \gamma^3W_{\text{in}}\left(x_1 - \sqrt{3}\bar{x}_2, p_1\right). \tag{F9}$$

This output state emerges, because in almost all cases, the feedforward operations turn mode 1 back into the initial state (in the case of finite squeezing, only up to some Gaussian-distributed excess noise depending on the degree of squeezing used for the encoding). The only case for which no correction occurs is when errors appear in every channel at the same time, at a probability of  $\gamma^3$ . In this case, the initial state remains uncorrected, with an  $x$ -displacement error of  $\sqrt{3}\bar{x}_2$ .

We see that a fidelity of  $1 - \gamma^3$  can be achieved, assuming  $\bar{x}_2 \gg 1$  (for smaller  $\bar{x}_2$ , the fidelity would even exceed  $1 - \gamma^3$ , but those smaller  $\bar{x}_2$  may be too hard to detect at the syndrome extraction, depending on the degree of squeezing, see below). Note that this result implies that the encoded scheme performs better than the unencoded scheme (direct transmission with  $F_{\text{direct}} = 1 - \gamma$ ) for *any*  $0 < \gamma < 1$ . In other words, by employing the quantum error correction protocol, the error probability can be reduced from  $\gamma$  to  $\gamma^3$ . The continuous-variable scheme in this model is more efficient than the analogous qubit repetition code and it does not require error probabilities  $\gamma < 1/2$  as for the case of qubit bit-flip errors<sup>12</sup>.

We may now consider two different regimes for the error displacements  $\bar{x}_2$ . First, the regime  $e^{-2r}/4 < \bar{x}_2 < 1/4$ , corresponding to small displacements below the shot noise limit; these can only be resolved provided the squeezing is large enough. In the limit of infinite squeezing  $r \rightarrow \infty$ , arbitrarily small shifts can be detected and perfectly corrected (with zero excess noise in the output states corresponding to unit fidelity).

Secondly, the regime  $\bar{x}_2 \gg 1$ . For these large shifts, even zero squeezing in the ancilla modes (i.e., vacuum ancilla states) is sufficient for error identification. Even with  $r = 0$ , the syndrome measurements still provide enough information on the location of the error and, to some extent, on the size of the error. We may refer to this kind of scheme as classical error correction (CEC), corresponding to the "classical cutoff" used as a classical boundary in the main body of the paper. This classical cutoff depends on the particular encoding and decoding circuit used; in the experiment, it is the same circuit as that employed for quantum error correction (neither of these are necessarily optimal).

CEC for large shifts  $\bar{x}_2 \gg 1$  (the regime of the experiment) works fairly well. In fact, the fidelity values without CEC drop to near-zero fidelities, as measured in the experiment,  $F < 0.007 \pm 0.001$ . Experimentally, this CEC is a highly nontrivial task and it is needed to achieve reasonable transfer fidelities. Nonetheless, the CEC scheme results in excess noise for the output state coming from the feedforward operations based on the fluctuating syndrome measurement results. By employing squeezed-state ancilla modes, this excess noise can

be reduced (down to zero for infinite squeezing). In this case, the scheme operates in the quantum regime. Significantly, in the experiment, non-commuting errors have been corrected, which means that CEC will always result in some excess noise. Although the margin of the demonstrated quantum error correction (on top of the CEC) is rather small, the experimental data provide clear evidence that CEC has been outperformed by the quantum scheme.